To appear in 1 December 2000 ApJ (Part 1)

Physical Conditions in Circumstellar Gas surrounding SN 1987A 12 Years After Outburst[1]

Stephen P. Maran[2], George Sonneborn[3], Chun S. J. Pun[3,4], Peter Lundqvist[5], Rosina C. Iping[3,6], Theodore R. Gull[3],

ABSTRACT

Two-dimensional spectra of Supernova 1987A were obtained on 1998 November 14-15 (4282 days after outburst) with the Space Telescope Imaging Spectrograph (STIS) on board the *Hubble Space Telescope* (*HST*). The slit sampled portions of the inner circumstellar ring at the east and west ansae as well as small sections of both the northern and southern outer rings. The temperature and density at these locations are estimated by nebular analysis of [N II], [O III], and [S II] emission line ratios, and with time-dependent photoionization/recombination models. The results from these two methods are mutually consistent. The electron density in the inner ring is ~ 4000 cm^{-3} for S II, with progressively lower densities for N II and O III. The electron temperatures determined from [N II] and [O III] line ratios are $\sim 11,000$ K and $\sim 22,000$ K, respectively. These results are consistent with evolutionary trends in the circumstellar gas from similar measurements at earlier epochs. We find that emission lines from the outer rings come from gas of lower density ($n_{\rm e} \lesssim 2000$ cm^{-3}) than that which emits the same line in the inner ring. The N/O ratio appears to be the same in all three rings. Our results also suggest that the CNO abundances in the northern outer ring are the same as in the inner ring, contrary to earlier results of Panagia et al. (1996). Physical conditions in the southern outer ring are less certain because of poorer

[1]Based on observations with the NASA/ESA *Hubble Space Telescope*, obtained at the Space Telescope Science Institute, which is operated by the Association of Universities for Research in Astronomy Inc., under NASA Contract NAS5-26555.

[2]Space Sciences Directorate, Code 600, NASA Goddard Space Flight Center, Greenbelt, MD 20771; stephen.p.maran@gsfc.nasa.gov

[3]Laboratory for Astronomy and Solar Physics, Code 681, NASA Goddard Space Flight Center, Greenbelt, MD 20771; pun@congee.gsfc.nasa.gov, george.sonneborn@gsfc.nasa.gov, gull@sea.gsfc.nasa.gov, rosina@taotaomona.gsfc.nasa.gov

[4]National Optical Astronomical Observatories, P.O.Box 26732, Tucson, AZ 85726

[5]Stockholm Observatory, SE-133 36, Saltsjöbaden, Sweden; peter@astro.su.se

[6]Department of Physics, Catholic University of America, Washington, DC 20064

signal-to-noise data. The STIS spectra also reveal a weak Hα emission redshifted by ~ 100 km s^{-1} at p.a. 103° that coincides with the recently discovered new regions that are brightening (Lawrence et al. 2000). This indicates that the shock interaction in the SE section of the inner ring commenced over a year before it became apparent in *HST* images.

Subject headings: supernovae: individual (SN 1987A) – supernova remnants – circumstellar matter

1. INTRODUCTION

Narrow emission lines (FWHM < 15 km s^{-1}) from nitrogen-enriched circumstellar gas around SN 1987A were first seen in the UV with the *International Ultraviolet Explorer (IUE)* satellite in 1987 May (Fransson et al. 1989), about 70 days after outburst. The circumstellar gas was ionized by the strong burst of extreme UV and soft X-ray radiation ($T_{\rm color} \sim 1 \times 10^6$ K, Blinnikov et al. 2000) produced when the shock front of the stellar explosion first broke through the surface of the star. The circumstellar gas was highly photoionized by the UV flash, reaching ioniziation level of at least N VI and O VII (Lundqvist & Fransson 1996). The subsequent cooling of the gas has produced the ring emission observed over the last thirteen years (except for the shock interaction emission, cf. §4.3). The UV emission lines peaked in brightness at $\sim$ day 400 when the light paraboloid swept through the whole inner ring region and these lines have been decaying since then (Sonneborn et al. 1997). As the emission is dominated by progressively lower density gas, the flux decay rate decreases with time. Optical emission lines (mainly [O III]) were first detected on about day 310 by Wampler & Richichi (1989). Subsequent ground-based imaging by Crotts, Kunkel, & McCarthy (1989) and Wampler et al. (1990) together with *Hubble Space Telescope* (*HST*) observations with the Faint Object Camera (Jakobsen et al. 1991) and Wide-Field/Planetary Camera 1 (Plait et al. 1995) showed that the brightest circumstellar material was distributed in a ring-like structure. Following the first *HST* Servicing Mission, the newly stigmatic *HST* revealed the fainter, more complex structure of the circumstellar material surrounding SN 1987A: an equatorial inner ring and two outer thin loops were clearly seen (Burrows et al. 1995).

The UV emission lines of the inner ring revealed that the SN 1987A circumstellar material has enhanced CNO abundances (N/C $\sim$ 29 and N/O $\sim$ 13 times solar, Fransson et al. 1989; Lundqvist & Fransson 1996; Sonneborn et al. 1997). This has proven to be one of the main observational constraints on the evolution of the supernova progenitor, implying that the star was in a post He-core burning phase at the time of the explosion (Podsiadlowski 1992). Photoionization/recombination modeling of the early UV line emission showed that the peak radiation temperature at the time of shock breakout was $\gtrsim 1 \times 10^6$ K (Lundqvist & Fransson 1996). This temperature is consistent with that predicted by the radiation-hydrodynamic modeling of the breakout (Ensman & Burrows 1992; Blinnikov et al. 2000). The similar decay times derived for the

different ionized states of the same element, such as N V and N III (Sonneborn et al. 1997), cannot be fitted with a single density model (Lundqvist & Fransson 1996). Instead, this result suggests that the inner ring consists of gas with a wide range of density $n_{\rm e} \sim 7 \times 10^3 - 4 \times 10^4$ cm^{-3}. In this non-equilibrium situation, gas of different density dominates the line emission at different times for a particular region in the ring because of the shorter recombination timescale for higher density gas (see Lundqvist & Fransson 1996 for a thorough discussion). In general, the line emission was first dominated by emission from the highest density gas, and later by successively lower density gas within the circumstellar ring.

The physical conditions of the inner ring have also been studied in optical wavelengths both from the ground and with *HST*. At the time of the earliest optical emission line observations, Wampler & Richichi (1989) derived a mean temperature of 45,000 – 75,000 K for electron densities below 10^5 cm^{-3} from the [O III] $\lambda\lambda$4959, 5007/λ4363 line ratio. Subsequent analyses (Khan & Duerbeck 1991; Menzies 1991; Wang 1991) of the [O III] line ratio up to $\sim$ day 1300 showed that the temperatures of the emitting O^{2+} ions remained at $\sim$ 30,000 K, while the [N II] $\lambda\lambda$6548, 6583/λ5755 line ratio indicated a temperature of $\sim$ 15,000 K. The electron density derived from the [S II] doublets λ6716/λ6731 was 10^4 cm^{-3}. From *HST*/Faint Object Spectrograph observations of the brightest location in the inner ring (p.a. = 300°) taken at day 2876, Lundqvist & Sonneborn (2000, henceforth LS00) derived the [N II] and [O III] temperatures to be $\sim 10,000$ K, and $\sim 27,000$ K, respectively, and a [S II] density of $\sim$ 9000 cm^{-3}. Combining with the *HST*/WFPC2 narrow band F648N ([N II]λ6583) and F502N ([O III]λ5007) observations, the average densities around the inner ring of the [N II]- and [O III]-emitting gas were determined to be $\gtrsim$ 4000 cm^{-3}, and $\sim$ 2300 cm^{-3}, respectively.

Compared to the inner ring, the physical conditions of the two thin outer rings have been much less studied because of their faintness (surface brightness of the outer rings are $\sim 5 - 15\%$ of that of the inner ring). Panagia et al. (1996) studied UV and optical *HST*/FOS spectra of the position on the northern outer ring that is coincident with the position of the SN 1987A debris. They concluded that while the ioniziation and temperature derived are similar to that of the inner ring, the outer ring gas studied is $\sim$ 3 times less CNO enriched than the inner ring, with a slightly lower electron density $n_{\rm e} \sim$ 800 cm^{-3}. The lower CNO abundances lead Panagia et al. to suggest that the outer ring gas materials were ejected by the SN 1987A progenitor $\sim 10^4$ years before that of inner ring gas. This result contrasts with recent kinematical studies of the three rings which indicate that all three rings are coeval, created $\sim$ 20,000 yr before the supernova explosion (Crotts & Heathcote 2000). As shown below in §4.2, the line emissions from the outer rings are highly time-dependent, and this effect may not have been sufficiently taken into account by Panagia et al. (1996).

In this paper we report long slit optical STIS spectroscopy of H I, [N II], [O III], and [S II] emission from the inner and outer circumstellar rings (§2). Multiple positions on the inner ring and the two outer rings have been observed and analyzed (§3). Ratios of these transitions form useful plasma diagnostics, with which we determine $n_{\rm e}$ and $T_{\rm e}$ of the emitting gas in the inner

(§4.1) and outer rings (§4.2). A preliminary version of this analysis was presented by Iping, Sonneborn, & Pun (1999). We constructed time-dependent photoionization/recombination models for both the inner and outer rings to check the consistency of the physical conditions derived from the line ratios. Finally, we report in §4.3 the detection of a Doppler-shifted Hα emission observed in the spectra, which can be attributed to the onset of interaction between the supernova debris and the ring at p.a. = 103°.

2. OBSERVATIONS

SN 1987A and its rings were observed with the *HST* Space Telescope Imaging Spectrograph (STIS) on 1998 Nov 14 and 15 (4282 days after core collapse). Medium resolution optical spectra taken with gratings G430M and G750M were obtained with a long, narrow slit ($52'' \times 0\farcs2$). The position of the STIS aperture is shown to scale in Figure 1(a). The center of the slit is close to the center of the debris and its orientation of position angle p.a. = 103° is close the major axis of the inner ring (p.a. $\sim$ 83°, Oppenheimer 1999). The spatial resolution in these spectral images is $\sim$ 1.4 – 1.6 pixels, or $0\farcs07$ – $0\farcs08$ (FWHM).

Crotts & Heathcote (2000; see also Cumming & Lundqvist 1997) have measured the expansion velocities of the inner equatorial ring (10.5 ± 0.3 km s^{-1}) and the two outer rings (26 km s^{-1}). The circumstellar rings remain spectrally unresolved in the STIS medium resolution grating modes, where the spectral resolution is $\sim$ 50 km s^{-1}. Multiple observations ($n = 4 - 5$) centered at dithered positions $0\farcs5$ apart along the slit were made with each grating setting. Cosmic rays and hot pixels were removed simultaneously when the dithered raw images were combined with the CALSTIS software developed by the STIS Investigation Definition Team at the Goddard Space Flight Center[7]. The grating settings used and the emission lines observed in each setting are listed in Table 1.

The long slit crossed portions of the inner ring near the east and west ansae. We refer to these positions in this paper as the "west" and "east" inner ring (WIR and EIR), as labelled in Figure 1. Assuming the ring is expanding instead of contracting, Crotts & Heathcote (1991) have shown that the northern side of the inner ring is inclined closer towards the observer. In that scenario, the WIR region is located closer towards the observer than the EIR region and emissions measured from the EIR originate from the inner ring $\sim$ 100 days *before* those received simultaneously from the WIR .

The slit also crosses the northern and southern outer rings each at two locations. However, only the emitting gas at the two intersection points farther from the supernova has sufficient brightness for our analysis. We refer to the sections of the outer rings studied in this paper as "north outer ring" (NOR) and "south outer ring" (SOR). Assuming the same geometry as the

[7]CALSTIS Reference Guide, http://hires.gsfc.nasa.gov/stis/software/doc_manuals.html

inner ring (see Figure 3 of Burrows et al. 1995 for an illustration), then the northern outer ring lies *farther* from the observer than the southern outer ring. And emissions from the NOR region originated ~ 900 days before those received simultaneously from the SOR region.

3. EMISSION LINE ANALYSIS

The inner and outer ring spectra were extracted from the STIS spectral images. A portion of the G750M spectral image is shown in Figure 1(b). The broad horizontal streak near the center is Hα emission from the supernova debris ($v_{\rm FWHM} \sim 2800$ km s^{-1}, Wang et al. 1996; Chugai et al. 1997). The spectra of the WIR and EIR were obtained by intergrating $8-12$ rows of the image where the ring flux is recorded. The extraction height varied slightly with the emission line species because of the different size and width of the circumstellar ring at each emission line (Sonneborn et al. 1997; Oppenheimer 1999). The Hα emission filling the length of the aperture in Figure 1(b) is from the diffuse LMC background and was removed by linear interpolation above and below the extracted rows. Diffuse LMC background emission is present in the Balmer lines and the [O III]$\lambda\lambda$4959, 5007 transitions. It is a source of systematic error for the ring flux measurements, especially for the outer rings, as described below. The integrated spectra were normalized to correct for the height of the extraction slit, that is, the number of rows integrated.

The flux of each spectral feature was measured by fitting a Gaussian to the line profile. The background level for each line was fit by a quadratic over a 12 to 25 Å ($40-50$ pixels) region of the spectrum centered on the feature being measured. The best fit was determined by minimizing the total χ^2 in which the Gaussian and background coefficients were free parameters. All the emission lines were fitted well by Gaussian profiles. We present the [O III]λ5007 emission profile fitting as an example in Figure 2. The reduced χ^2, or the total χ^2 divided by the number of degrees of freedom, should be 1.0 for a perfect fit. The reduced χ^2 of our line fits were all within the range $0.7-2.0$. For each feature, the line flux and its error were computed from the best fit parameters and their associated uncertainties. The statistical errors of all the line fluxes were adjusted so that the reduced χ^2 for all fits is 1.0.

As mentioned above, diffuse emission from the 30 Doradus region of the LMC filled the slit and contributed to the error of flux measurements of the rings. The diffuse background flux varied by a factor of ~ 2 along the slit in the immediate vicinity ($\pm 2\farcs5$) of the supernova. The diffuse background level at a given position along the slit, determined by linear interpolation, could be measured only to an accuracy of $\sim 15\%$. For the inner ring, the subtracted background was only a small fraction of the line emission ($<5\%$ for Hα and $<10\%$ for [O III]λ5007) and therefore the additional errors caused by background subtraction were negligible. On the other hand, the diffuse background levels were comparable to those of the measured outer ring fluxes for Hα and [O III]$\lambda\lambda$4959, 5007. The additional uncertainties due to the background subtraction were larger for the SOR than the NOR because the lower fluxes of the SOR. We included the extra uncertainty due to this background in the calculations of the total error in the outer ring flux measurements.

Results of the emission line flux measurements, normalized to Hα, are tabulated in Table 2. For the outer rings, the tabulated errors were determined by adding the uncertainties in the background flux and the statistical uncertainties in quadrature. As discussed in §4.3, the EIR Hα emission overlaps with a weak redshifted high velocity emission originating from the interaction between the supernova debris and inner ring. The EIR Hα flux listed in Table 2 has been corrected for the small contribution from this "hotspot." The tabulated fluxes are dereddened with E$(B-V)$ of 0.16 (Fitzpatrick & Walborn 1990) and the extinction law of Cardelli, Clayton, & Mathis (1989) with an assumed R_V of 3.1. The differences between the LMC extinction law and the Galactic law are negligible in the optical at low color excess and have been ignored in our analysis (Fitzpatrick 1999).

4. RESULTS

4.1. Inner Ring

Forbidden line ratios were used to estimate the physical conditions in the circumstellar rings. We updated the methodology described by Osterbrock (1989) with multilevel model atoms and with more recent atomic data. We included five levels for S II, whereas for N II and O III we used six-level atoms. We included O III atomic data from Aggarwal (1993) and Galavis, Mendoza, & Zeippen (1997), the results of Stafford et al. (1994) and Galavis et al. (1997) for N II, and results from Keenan et al. (1993) and Ramsbottom, Bell, & Stafford (1996) for S II. Previous studies established that gas with the range $n_{\rm e} \sim 10^3 - 10^4$ cm^{-3} are present in the inner ring (Fransson et al. 1989; Lundqvist & Fransson 1996; Sonneborn et al. 1997). Within this density range, the [N II] and [O III] line ratios,

$$R(\text{N II}) = \frac{(I(\lambda 6548) + I(\lambda 6583))}{I(\lambda 5755)} \quad \text{and}$$

$$R(\text{O III}) = \frac{(I(\lambda 4959) + I(\lambda 5007))}{I(\lambda 4363)},$$

are not very sensitive to electron densities $n_{\rm e}$ and provide a good measure of the electron temperature $T_{\rm e}$. Similarly, the ratio

$$R(\text{S II}) = \frac{I(\lambda 6716)}{I(\lambda 6731)}$$

is a good diagnostic of $n_{\rm e}$ with a weak dependence on $T_{\rm e}$.

The assumption inherent in the nebular analysis technique is that the gas considered has a constant $n_{\rm e}$ and $T_{\rm e}$ within the volume. This condition is not met in the SN 1987A circumstellar gas and therefore the physical conditions derived below in §4.1.1 with the line ratios represent only an average range of $n_{\rm e}$ and $T_{\rm e}$ that can be present in the gas. The situation is further complicated by the uncertainty in the geometry of the circumstellar gas. LS00 showed that the same [N II] and

[O III] line fluxes observed would imply a higher [N II]- and [O III]-emitting gas density for the case of a ionization-bounded ring than for the density-bounded, or, "truncated," case. As a consistency check of the results obtained from the nebular analyses, we therefore constructed time-dependent photoionization/recombination models below in §4.1.2 which incorporated the geometry effect and calculated $n_{\rm e}$ and $T_{\rm e}$ self-consistently.

4.1.1. Temperature and Density from plasma diagnostics

In Figure 3, we plotted the relationship between the line ratio R(N II) and $T_{\rm e}$ in our atomic model. Our calculated R(N II) values were very similar to those computed by McKenna et al. (1996), as the only difference is that we used newer transition probabilities (Galavis et al. 1997). The electron densities considered in Figure 3, $n_{\rm e} = 1000$ and 4000 cm^{-3}, were the lower and upper density limits respectively, of the [N II] emitting gas based on the modeling results of [N II]λ6583 *HST*/WFPC2 inner ring images up to day 3478 at the EIR and WIR positions (LS00). The observed values of R(N II) for the WIR and EIR regions, as well as the derived range on $T_{\rm e}$ as constrained by the density range under consideration, are also shown in Figure 3 and listed in Table 3.

For the [O III] temperature, we calculated the relationship between the line ratio R(O III) and $T_{\rm e}$ for electron densities of 800 and 2400 cm^{-3}. The range of $n_{\rm e}$ considered for [O III] was slightly lower than that for [N II], as suggested by an analysis of [O III]λ5007 *HST*/WFPC2 images (LS00). R(O III) and $T_{\rm e}$(O III) are also listed in Table 3. The uncertainty in the derived [O III] temperature was larger than that for [N II] because the [O III]λ4363 emission was very weak. We were only able to derive a lower limit of the temperature for the EIR region and we listed the 1-σ lower limit in Table 3.

We calculated the relationship between the line ratio R(S II) and $n_{\rm e}$ for electron temperatures 5000 and 10,000 K. The temperature limits chosen were based on the results from an analysis of the day 2876 0.″45 diameter aperture *HST*/FOS spectrum centered at p.a.=300° of the inner ring (LS00). The ring subsection sampled in the FOS spectrum lies close to the WIR region that is studied in this work. The derived range of the [S II] density from R(S II) is also listed in Table 3.

The temperatures measured here for the WIR and EIR are close to those reported by LS00 for the inner ring at p.a. = 300°, which were $\sim 10,000$ K for [N II], and $\sim 27,000$ K for [O III]. The slightly higher [N II] temperature found at p.a. = 283° (EIR) compared with p.a. = 103° (WIR) appears to be real. This indicates that the [N II]-emitting gas could be slightly denser at p.a. = 103°, which is consistent with the ongoing trend observed since day 3270 from *HST*/WFPC2 imaging (LS00). As discussed below, the density difference does not have to be large.

4.1.2. Consistency check from modeling

We constructed photoionization/recombination models for the inner ring to check the results derived from the plasma diagnostic line ratios in the previous section. The code for the model and the input elemental abundances were the same as those used in Lundqvist (1999), except for the Si abundance which was reduced to Si/H $= 1 \times 10^{-5}$ (cf. LS00). Recently, the spectrum from the supernova breakout has been re-calculated with the multienergy group radiation hydrodynamics code *STELLA* and it is in good agreement with the early (up to $\sim$ day 150) optical/UV light curves of SN 1987A (Blinnikov et al. 2000). That result will be used later in a more thorough investigation of the rings (P. Lundqvist, in preparation). Here we used the model "*500full1*" burst spectrum of Ensman & Burrows (1992), which was accurate enough for our purposes.

Guided by the densities derived from the [S II] line ratio, we computed models for atomic densities in the range $500 - 5000$ cm^{-3}. The resulting electron density would be $\sim 17\%$ higher if the gas is fully ionized, but is probably the same as the atomic density in the epoch that we are considering. The inner radius of the ring is assumed to be 6.3×10^{17} cm, as in Lundqvist & Fransson (1996). We modeled the temperature sensitive ratios R(N II) and R(O III) as a function of atomic density (Figure 4). Although the light travel time differences are not as important across the inner ring as for the outer rings (see below), we included this effect in our models. The line ratios were calculated for two cases: an ionization-bounded model, and a model where we simulated a density-bounded situation by including only the innermost 25% of the ionized gas, which we referred to as "25% truncation". R(N II) quickly increases from low values ($\sim 15 - 25$) to very large values ($\gtrsim 100$) at a density in the range $1000 - 3000$ cm^{-3}, the exact value of which depends on the degree of truncation. For example, R(N II) $= 50$ is reached at ~ 1700 cm^{-3} for the 25% truncation model, and at ~ 2700 cm^{-3} for the ionization-bounded case.

In our model, the observed R(N II) ratios in the inner ring are actually very sensitive to density. This is contrary to what is expected in the standard nebular analysis where R(N II) is used to determine electron temperature because it is relatively insensitive to variations in electron densities. The reason for this discrepency is that the temperature of the emitting gas at a specific epoch in the SN 1987A inner ring depends on the density of the gas, which drops faster for the higher density component. This translates directly into different line ratios for different density components within the gas. Only models with an average temperature of the line emitting gas similar to the temperature given by the nebular analysis will give the correct line ratio.

On the other hand, the degree of truncation has only minor effects on the dependence of the [O III] line ratio with density. Assuming these two cases represent the range of possible models (LS00), we derived the [N II] density of the WIR region to be $2400 - 3500$ cm^{-3} and the [O III] density to be $1400 - 2100$ cm^{-3}. For the EIR region, the corresponding numbers were $1700 - 3000$ cm^{-3} and $\lesssim 2100$ cm^{-3}, respectively. This suggests that the [S II], [N II], and [O III] emission come from regions of progressively lower density, consistent with the findings of LS00. Moreover, the densities derived in this paper (day 4282) are somewhat lower than those in

LS00 (day 3000). This is consistent with the trend that gas components of progressively lower density dominate the emission for a particular transition at later and later times. The higher the ionization potential of a line, the lower the density of the gas that emits it at a specific epoch. This has the interesting effect that the density components dominating the [O III] emission in the epoch studied in LS00 ($\sim$ day 3000), could be the same as those dominating the [N II] emission in this analysis (day 4282).

4.2. Outer Rings

With the emission from the outer rings much weaker than that from the inner ring, the uncertainties in the outer ring fluxes are much larger than those for the inner ring (cf. Table 2). Both [N II]λ5755 and [O III]λ4363 are absent, or very close to the noise limit, in our data for the outer rings. Therefore we cannot obtain a meaningful estimate of the electron temperature directly from the line ratios R(N II) and R(O III). The [S II]$\lambda\lambda$6716, 6731 lines, on the other hand, are both relatively strong and do not suffer from systematic errors in background subtraction (cf. §3). Using the R(S II) method (§4.1), we arrived at a 1-σ upper limit on the electron density of the NOR (SOR) of $n_{\rm e} \lesssim 2200$ (1600) cm^{-3}, allowing for a $T_{\rm e}$ between 5000 K and 10000 K. The derived outer ring densities are about a factor of two lower than the inner ring. The slightly higher electron density for the NOR, which lies further away from us than the SOR, may indicate that the effect of light travel time is important for the outer rings.

As a consistency check, we also computed photoionization/recombination models for the outer rings to model the observed [S II]/Hα, [N II]/Hα, and [O III]/Hα flux ratios. The code and elemental abundances were the same as those used for the inner ring analysis (§4.1.2). We adopted 2×10^{18} cm as the distance of the outer rings from the supernova. This means that there is a ~ 900 day difference in age of the emission from the observed positions on the SOR and NOR (§2). We took this different light travel time into account in our models. Guided by the densities derived from R(S II) for the outer rings, we ran models for atomic densities in the range $500 - 2000$ cm^{-3}.

As discussed in Lundqvist & Fransson (1996), the degree of ionization of the circumstellar gas after shock breakout is sensitive to the distance of the gas to the supernova. It is particularly important for the "*500full1*" model by Ensman & Burrows (1992) because of the smaller number of high energy photons in the burst spectrum. At a distance 3.2 times farther away from the supernova than the inner ring, the inner part of the outer rings was dominated by C IV, N IV, and O IV shortly after breakout, instead of the higher ionized species such as N VI, and O VII that were present in the inner ring, at the density range that we are considering (Lundqvist & Fransson 1996). We calculated that the maximum temperature reached in the outer rings from the initial UV flash was only $\sim 7.8 \times 10^4$ K, a factor of ~ 2 smaller than that in the inner ring. At $\sim$ day 3500, roughly the mean epoch of emission for the SOR and NOR positions we observed, for an atomic density of 1400 cm^{-3}, the maximum temperature in the outer rings would be $\sim 1.8 \times 10^4$ K, and the dominant ions C II, N II, and O II. For a density of 500 cm^{-3}, the dominant ions would

be C III, N III, and O III instead, and the temperature would be in the range $(1.0 - 4.5) \times 10^4$ K. In Figure 5 we show the modeled emissions in [S II]$\lambda\lambda$6716, 6731, [N II]$\lambda\lambda$6548, 6583, and [O III]$\lambda\lambda$4959, 5007, normalized to Hα as functions of atomic density. Similar to the inner ring, we considered two limiting cases for the outer ring modeling: an ionization-bounded model and a 25% truncation model (cf. §4.1.2). We plotted the observed normalized fluxes [N II]/Hα, [O III]/Hα, and [S II]/Hα for both the SOR and NOR regions for comparison with the models.

For the NOR, the density implied by the [S II]/Hα flux ratio in the model ($1000 - 2000$ cm^{-3}) was indeed consistent with that indicated by the line ratio R(S II) in Table 3. We concluded that the observed NOR [S II] lines could be interpreted with a model where the input S abundance was the same as that of the inner ring, i.e., S/H $\sim 6 \times 10^{-6}$. Similarly, Figure 5 also suggested that the NOR [N II] and [O III] emissions were consistent with a model where the emitting gases ($n_{\rm e} \sim 1300$ cm^{-3}) were less dense than those in the inner ring, but with the same N and O abundances. Our results favor a coeval scenario for the inner and outer rings, as argued for in Crotts & Heathcote (2000). Due to large uncertainties in the measured fluxes, caused largely by uncertainties in the background subtraction, we were unable to determine whether the NOR is ionization- or density-bounded.

For the SOR, the [S II] density estimate from our model ($700 - 1500$ cm^{-3}) was again consistent with that from the R(S II) calculations. However, even for the 25% truncation model, the modeled [N II] emission from the SOR is $\gtrsim 10\%$ higher than the observed value. In fact, only truncated models (and possibly with even more truncation, such as a 10% truncation model) can possibly fit the results, if we assume that the N abundance in the SOR is similar to that in the inner ring. The SOR [N II] emission then implies a density $\lesssim 1000$ cm^{-3}. However, the [O III] density inferred for the SOR in Figure 5 is ~ 1500 cm^{-3}. This result, that the [O III]-emitting region has higher density than that of the [N II]-emitting region in the SOR, is opposite to what is expected (cf. §4.1.2). We note though, that the modeled ratio of [N II]/[O III] is the same as the observed SOR value for a density of ~ 1000 cm^{-3}, which could either indicate a lower overall metal abundance in the SOR than in the NOR (although with similar relative abundances of N and O), or that the adopted value of the LMC Hα background in the SOR which we subtracted was too low. As described in §3, the SOR region is more vulnerable to background subtraction errors than the NOR because it is fainter. The observed SOR [N II]/Hα flux ratio could be brought to agreement with the model if the real LMC Hα background at the position of SOR was $\sim 10\%$ larger than the value we have adopted. Despite this problem, we note that the [O III]/Hα ratio is very sensitive to the density, placing a lower limit on the density of the emitting regions in both of the outer rings at ~ 1000 cm^{-3}.

The densities we derive, $\sim 1000 - 2000$ cm^{-3}, are somewhat larger than estimated by Panagia et al. (1996), who found 800 cm^{-3} on day 2887 for a single position of the northern outer ring. This is not necessarily a real contradiction, since the UV lines studied by Panagia et al. probe mainly hot gas ([N III], C III], [O III]), which, in order to stay hot at these late epochs cannot be dense. However, we do not feel that their result, that the N abundance in the outer rings is a

factor of $\sim 2-3$ smaller than the inner ring, is conclusive. A time dependent, and self-consistent analysis is required to study the extreme non-equilibrium conditions encountered in the rings at late epochs.

We close this discussion by noting that creating a density of $\sim 1000-2000$ cm^{-3} at the position of the outer rings poses a real challenge to models of the formation of the ring system. For example, it is a factor ~ 10 higher than indicated by the models of Blondin & Lundqvist (1993) and Martin & Arnett (1995). Multidimensional models including photoionization by the progenitor have not yet demonstrated an improvement of this situation (e.g., Chevalier 2000). High quality spectra with good S/N are needed to accurately determine the temperature, ionization and abundances of the gas in the outer rings.

4.3. Spot 3 discussion

The first evidence for the collision between the supernova ejecta and the inner circumstellar ring came in 1997 April from the STIS observations of a Hα emission feature blueshifted up to ~ 250 km s^{-1} that was projected near the inside edge of the spectral image of the ring (Sonneborn et al. 1998). Subsequent photometric observations with *HST*/WFPC2 (Garnavich et al. 2000a) and spectroscopic observations with STIS (Michael et al. 2000) of this hotspot (Spot 1) demonstrate continued brightening plus emissions in other species such as [O I], [N II], and [O III]. The appearance of Spot 1 was explained as the result of the collision of the outer shock from the SN 1987A debris with a dense knot of gas protruded inward towards the supernova from the ring. Additional spots were predicted to appear once the debris collides with the rest of the ring. The presence of a new source of radiation was first reported in the CTIO He I 1.08μm image in 1999 December 25 by Bouchet et al. (2000). Subsequent STIS (Maran, Pun, & Sonneborn 2000) and WFPC2 (Garnavich, Kirshner, & Challis 2000b) imaging showed that 5 additional bright spots have developed around the inner ring. In Figure 1(b), we point out a redshifted component in Hα in the G750M (6581) spectral image which was first identified in this data by Lawrence & Crotts (2000). This high-velocity Hα emission originates from the inner edge of the EIR region. No similar Doppler-shifted emission is observed in our data for any other species. The position of this redshifted Hα flux coincides with that of Spot 3 (or HS2-106, using the nomenclature of Lawrence et al. 2000), one of the recently discovered new regions of brightening on the SN 1987A inner ring reported by Garnavich et al. (2000b). Measurements of Spot 3 in the 2000 February 2 (day 4727) WFPC2 images gave a position of $0\farcs70$ away from the center of the SN 1987A debris and a position angle of 106°. This is the start of the full scale collision between the supernova ejecta and the inner circumstellar ring, as also pointed out by Lawrence et al. (2000).

The combined Hα spectrum of the Spot 3 and the overlapping portion of the EIR is extracted in a similar manner as that described in §2, except that fewer rows ($n = 4$) are integrated for the output spectrum. The extracted Hα profile for Spot 3 and the ring is shown in Figure 6. Redshifted emission from Spot 3 is clearly observed up to $\sim +175$ km s^{-1} while the blueshifted component

cannot be identified because the extracted spectrum is dominated by the EIR flux that fills the width of the aperture between ± 100 km s^{-1}. We fitted the rest of the Hα emission with a Gaussian function and a linear background. The best-fit Gaussian is shown by the dotted line in Figure 6. The Hα flux from Spot 3 derived from the best-fit parameters is $(8 \pm 4) \times 10^{-17}$ ergs cm^{-2} s^{-1} (no reddening correction). With only the redshifted profile available for fitting, the FWHM of the emission is poorly constrained to be 100 ± 50 km s^{-1}. On the other hand, the emission-line width of Spot 1 in Hα measured from much better S/N STIS observations gives a FWHM width of 253 ± 4 km s^{-1} (Michael et al. 2000). Subsequent monitoring of the Spot 1 Hα radiation profile suggests that the width of the radiation remains constant with time (C.S.J. Pun, in preparation). If we assume that the intrinsic width of Spots 1 and 3 are identical, then we expect the *observed* FWHM of the Spot 3 profile to be 195 km s^{-1}, after correcting for the different position angles of the two spots on the ring. With the profile width fixed, we determined a more accurate Spot 3 flux to be $(2.0 \pm 0.6) \times 10^{-16}$ ergs cm^{-2} s^{-1} (no reddening correction). The best fit profile is shown with dashed line in Figure 6. The portion of this radiation ($\sim$68%, or 1.4×10^{-16} ergs cm^{-2} s^{-1}) that lies within the $0\farcs2$ aperture has been removed for the determination of the EIR Hα inner ring flux (cf. §3). The Spot 3 flux measured in this paper was consistent with the value previously reported using the same data by Lawrence et al. (2000).

Using the CALCPHOT task in the SYNPHOT package of the STSDAS data reduction software, we converted the Spot 3 flux in 1998 November to an equivalent STMAG magnitude of 21.7 (0.4). If we assume the rate of brightness increase for Spot 3 is the same as that of Spot 1, 2.09 ± 0.11 mmag day^{-1} (Garnavich et al. 2000a), then the extrapolated brightness for Spot 3 on day 4727 will be 20.7 (0.4). Our predicted flux was ~ 1 mag fainter than the measured WFPC2 Hα photometric result of 19.6 (1.6×10^{-15} ergs cm^{-2} s^{-1}) on day 4727 (Garnavich et al. 2000b), probably caused by the fact that Spot 3 is not centered within the STIS aperture in our data.

Finally, we comment on the monitoring of the interaction between the SN 1987A debris and the circumstellar ring. While difference imaging in Hα, [N II], and He I 1.083μm, where the newly-formed spots have the greatest contrast above the equatorial inner ring, may be a sensitive technique (Lawrence et al. 2000), it is susceptable to problems in separating the flux from the newly formed spots from the noisy background. It is not surprising that by separating the emission of the slow-moving ring ($v \sim 10$ km s^{-1}) from that of the interacting spots ($v \sim 250$ km s^{-1}), radiation from Spot 3 could be detected in the STIS data at least one year before discovery by imaging, and over six months before it could be identified in pre-discovery images. This indicates that high resolution spectroscopic monitoring provides the best technique for discovering new areas of shock interaction in SN 1987A.

We are grateful to Peter Garnavich and Arlin Crotts for useful discussions. We thank Don Lindler, Phil Plait, and the Goddard STIS team for their help with data reduction, and the Supernova Intensive Study (SINS, PI: Robert Kirshner) team for access to their unpublished data. This work was supported by NASA Guaranteed Time Observer funding to the STIS Science Team

(PI: Bruce Woodgate). C.S.J.P. acknowledges funding by the STIS IDT through the National Optical Astronomy Observatories. P.L. acknowledges support from the Swedish Natural Science Research Council and the Swedish National Space Board.

Table 1. 1998 November 14 (day 4282) STIS Observations

Gratings	Wavelength Range (Å)	Exposure time (sec)	Emission lines observed
G750M (6581)	6295 – 6867	4750	[O I] 6300,64, Hα, [N II] 6548,83, He I 6678, [S II] 6716,31
G750M (5734)	5448 – 6020	5250	[N II] 5755, He I 5876
G430M (4961)	4818 – 5104	5750	Hβ, [O III] 4959, 5007
G430M (4451)	4308 – 4594	7000	Hγ, [O III] 4363
G430M (3423)	3280 – 3566	7000	···

Table 2. Normalized and dereddened emission line fluxes from the inner and outer rings

Ion	λ (Å)	WIR[a]	EIR[b]	NOR[c]	SOR[d]	Extinction Correction[e]
Hγ	4340.46	0.155 ± 0.011	0.172 ± 0.014	0.333 ± 0.176	0.186 ± 0.103	1.850
[O III]	4363.21	0.015 ± 0.006	0.021 ± 0.015	···	···	1.843
Hβ	4861.32	0.352 ± 0.013	0.319 ± 0.019	0.514 ± 0.175	0.460 ± 0.206	1.702
[O III]	4958.91	0.136 ± 0.011	0.140 ± 0.016	0.284 ± 0.113	0.165 ± 0.110	1.679
[O III]	5006.84	0.384 ± 0.015	0.444 ± 0.024	0.932 ± 0.290	0.344 ± 0.227	1.668
[N II]	5754.59	0.060 ± 0.006	0.085 ± 0.012	0.198 ± 0.096	···	1.543
He I	5875.65	0.054 ± 0.004	0.056 ± 0.008	···	···	1.528
[O I]	6300.30	0.154 ± 0.007	0.144 ± 0.012	···	···	1.480
[O I]	6363.78	0.061 ± 0.006	0.044 ± 0.006	···	···	1.474
[N II]	6548.05	1.189 ± 0.024	1.202 ± 0.045	1.062 ± 0.216	0.395 ± 0.122	1.454
Hα	6562.82	1.000	1.000	1.000	1.000	1.453
[N II]	6583.45	3.534 ± 0.084	3.486 ± 0.143	2.476 ± 0.470	1.399 ± 0.378	1.451
He I	6678.15	0.014 ± 0.004	0.012 ± 0.005	···	···	1.441
[S II]	6716.44	0.208 ± 0.006	0.201 ± 0.012	0.261 ± 0.073	0.243 ± 0.086	1.437
[S II]	6730.82	0.347 ± 0.009	0.338 ± 0.018	0.210 ± 0.086	0.196 ± 0.072	1.436

[a]Dereddened WIR H$\alpha = (71.56 \pm 0.95) \times 10^{-16}$ ergs cm^{-2} s^{-1}

[b]Dereddened EIR H$\alpha = (41.12 \pm 1.16) \times 10^{-16}$ ergs cm^{-2} s^{-1}

[c]Dereddened NOR H$\alpha = (3.59 \pm 0.51) \times 10^{-16}$ ergs cm^{-2} s^{-1}

[d]Dereddened SOR H$\alpha = (4.01 \pm 0.64) \times 10^{-16}$ ergs cm^{-2} s^{-1}

[e]E$(B-V) = 0.16$, and the extinction correction law of Cardelli et al. (1989) and $R_V = 3.1$.

Table 3. Plasma Diagnostics

Parameter	WIR	EIR	NOR	SOR
R(N II)	78.6 ± 8.4	55.0 ± 7.4	···	···
$T_{\rm e}$(N II) (K)	10300^{+700}_{-600}	12100^{+1200}_{-900}	···	···
R(O III)	34.1 ± 12.6	27.7 ± 19.3	···	···
$T_{\rm e}$(O III) (K)	21400^{+9400}_{-3700}	>17700	···	···
R(S II)	0.599 ± 0.020	0.596 ± 0.041	1.16 ± 0.45	1.20 ± 0.42
$n_{\rm e}$(S II) (cm^{-3})	3880^{+1150}_{-1060}	4000^{+2410}_{-1510}	<2200	<1600

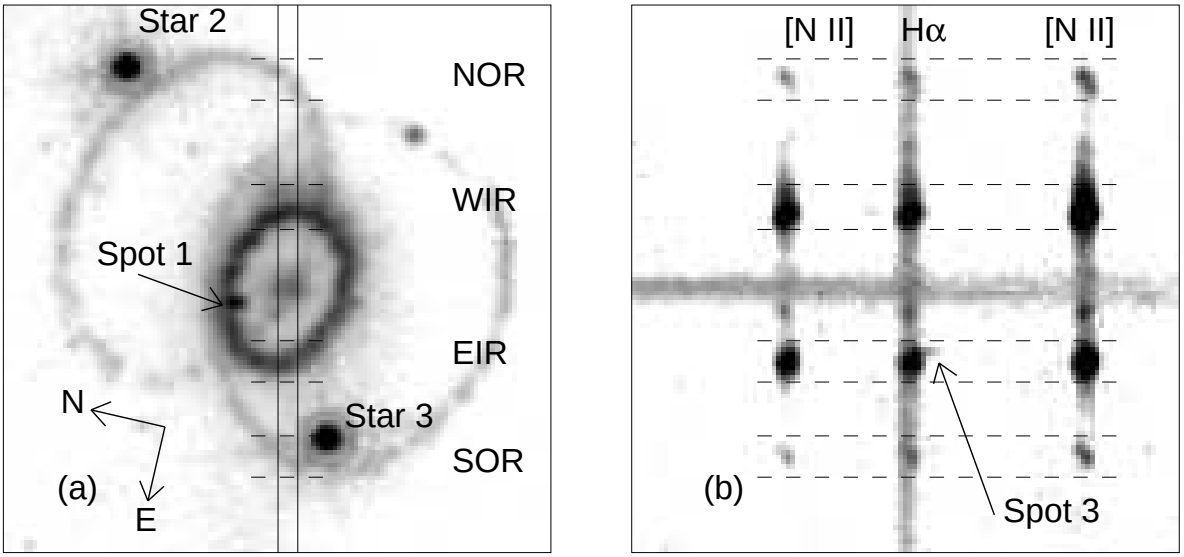

Fig. 1.— (a) The size and orientation of the STIS aperture are shown on a 1999 January WFPC2 image of SN 1987A. The image size is 5.″8 square. The regions of the west inner ring (WIR), east inner ring (EIR), north outer ring (NOR), and south outer ring (SOR) spectra extractions are also shown by horizontal dashed lines; (b) Section of the STIS G750M (6581) spectral image showing the emission from Hα and [N II]$\lambda\lambda$6548, 6583. The spatial scale is identical to (a). The dashed lines show the spectral extraction regions for the inner and outer ring spectra. The arrow points to the redshifted Hα emission that indicates the presence of shock interaction. Its position also indicates that this emission originates on the inner edge of the ring.

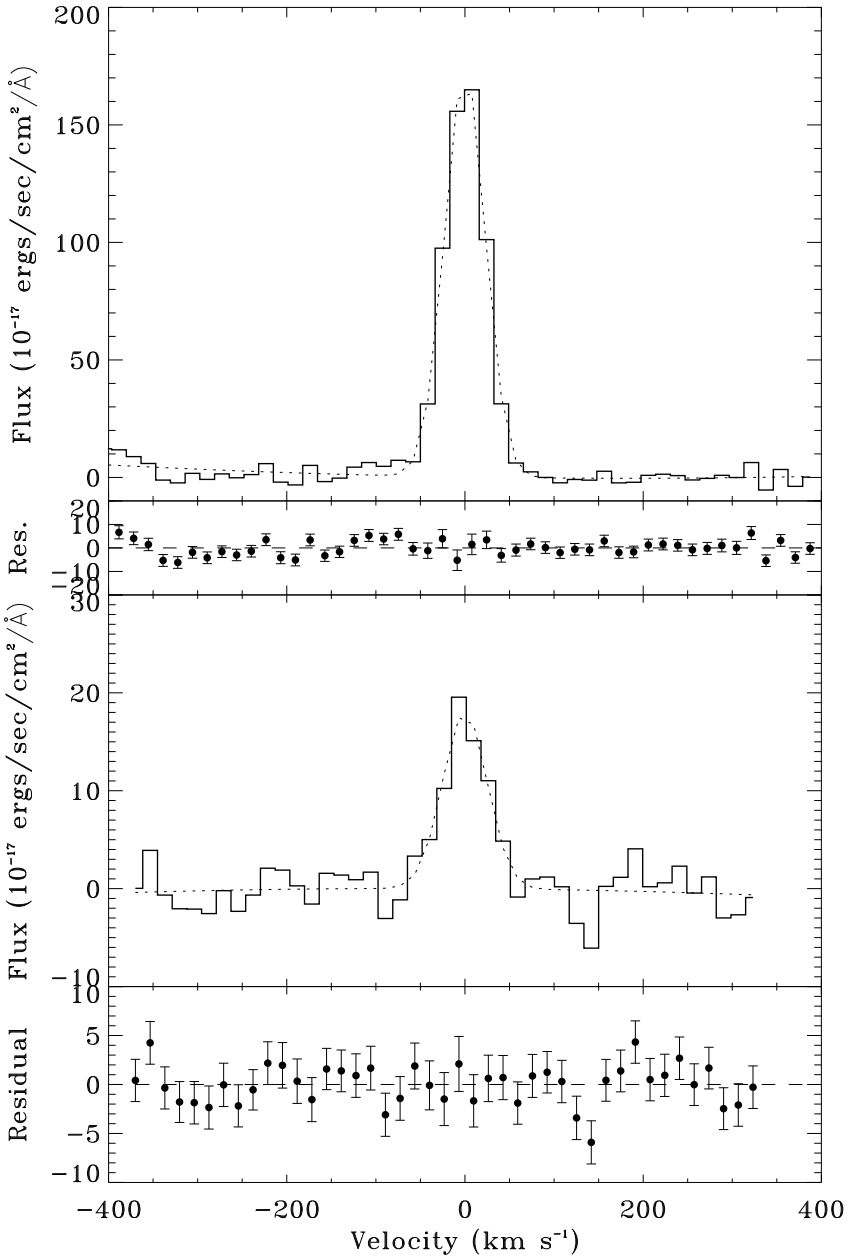

Fig. 2.— Sample gaussian profile fitting for the [O III] λ5007 emission. The top panel shows the [O III] λ5007 emission from the EIR region (thick line) along with the best χ^2 fit (broken line). The reduced χ^2 of the fit is 1.9. The bottom panel shows the [O III] λ5007 emission from the SOR region (thick line) along with the best χ^2 fit (broken line). The reduced χ^2 of the fit is 1.0.

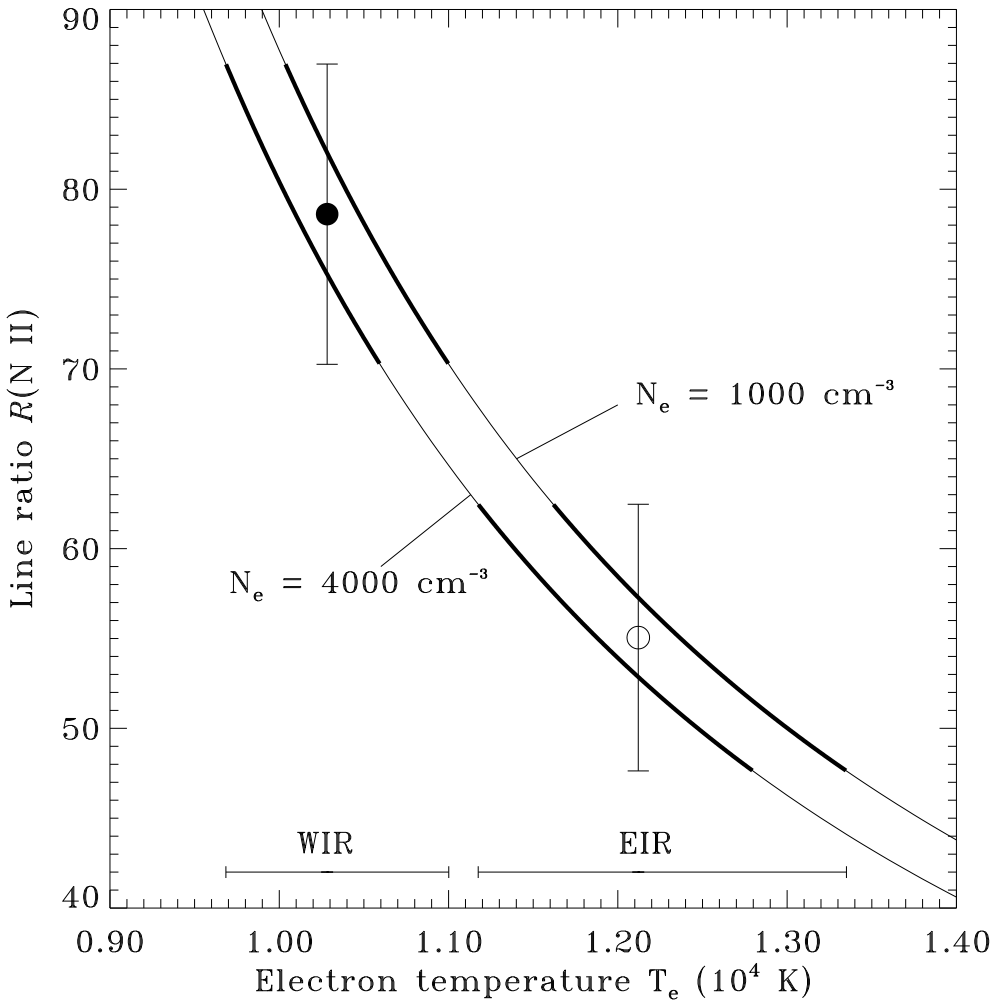

Fig. 3.— The theoretical [N II] line ratio (λ6548 + λ6583)/λ5755 as a function of electron temperature is shown for two electron densities (1000 and 4000 cm^{-3}). The observed [N II] line ratios for the WIR (filled circle) and EIR (open circle) inner ring areas and the implied electron temperatures for the two regions are also shown.

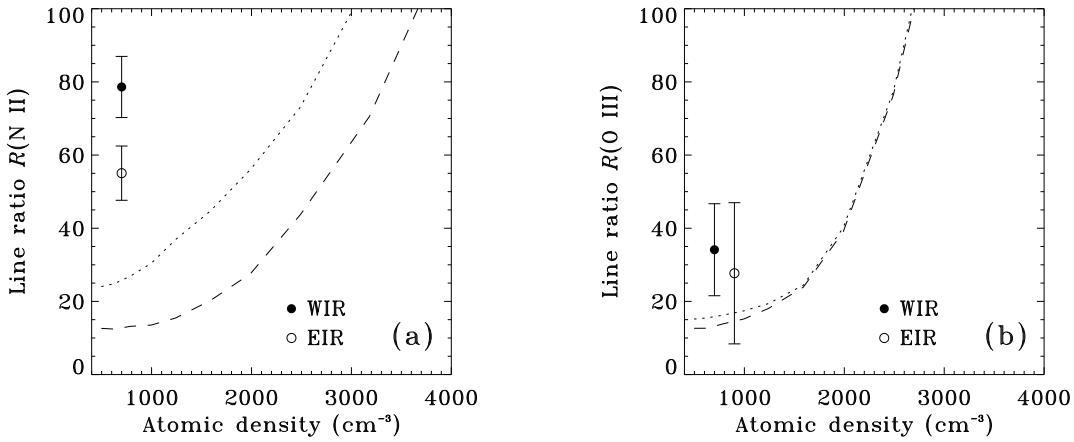

Fig. 4.— (a) The computed model [N II] line ratio (λ6548 + λ6583)/λ5755 is plotted against the atomic density for the SN 1987A inner ring gas with an ionization bounded model (dash) and a 25% truncation density bounded model (dotted); (b) Similar as (a), for the model [O III] line ratio (λ4959 + λ5007)/λ4363. The measured [N II] and [O III] line ratios from the west (WIR, filled circle) and east (EIR, empty circle) inner ring areas are also shown.

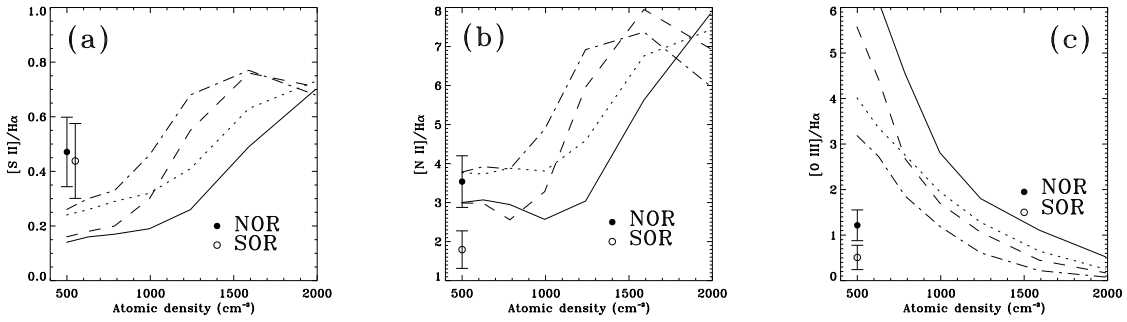

Fig. 5.— (a) The computed model [S II] line flux (λ6716 + λ6731)/Hα is plotted against the atomic density for the NOR gas with an ionization bounded model (dotted) and a 25% truncation density bounded model (solid), along with the model line fluxes for the SOR gas with the ionization bounded model (dot-dash) and the 25% truncation model (dash); (b) Similar as (a), for the model [N II] line flux (λ6548 + λ6583)/Hα; (c) Similar as (a), for the model [O III] line flux (λ4959 + λ5007)/Hα; The measured line fluxes from the northern (NOR, filled circle) and southern (SOR, empty circle) outer ring areas are also shown.

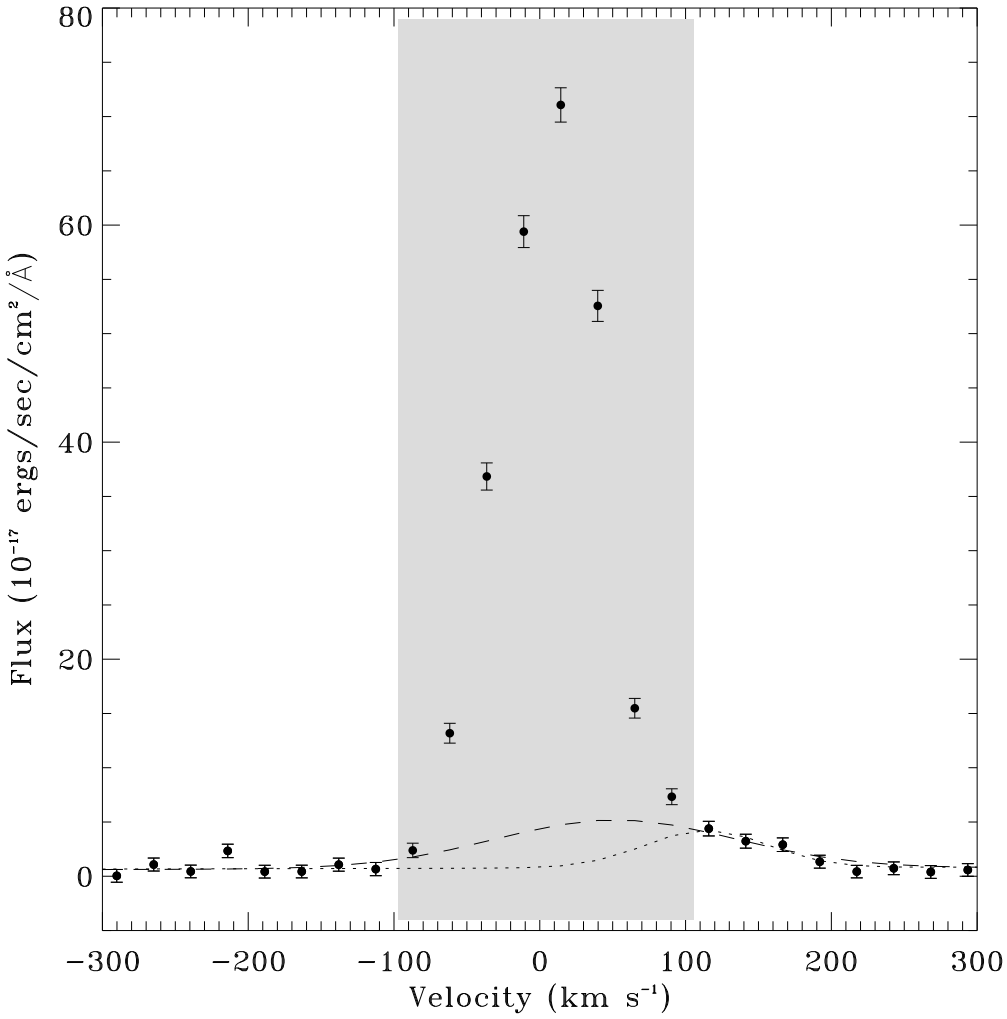

Fig. 6.— The Hα profile from the east section of the inner ring. The shaded area represents the region where the radiation is dominated by the ring and not used for the fitting. The redshifted emission from Spot 3 is fitted by a Gaussian for both the cases where the width of the emission is a free parameter (dot) and where the FWHM of the emission is set to be 195 km s^{-1} (dash).

REFERENCES

Aggarwal, K. M. 1993, ApJS, 85, 197

Blinnikov, S. I., Lundqvist, P., Bartunov, O. S., Nomoto, K., & Iwamoto, K. 2000, ApJ, 532, 1132

Blondin, J. M., & Lundqvist, P. 1993, ApJ, 405, 337

Bouchet, P., Lawrence, S., Crotts, A., Sugerman, B., Uglesich, R., & Heathcote, S. 2000, IAU Circular No. 7354

Burrows, C. J., et al. 1995, ApJ, 454, 680

Cardelli, J. A., Clayton, G. C., & Mathis, J. S. 1989, ApJ, 345, 245

Chevalier, R. A. 2000, in SN 1987A: Ten Years After, eds. M. Phillips & N. Suntzeff, A.S.P Conference Series (in press)

Chugai, N. N., Chevalier, R. A., Kirshner, R. P., & Challis, P. M. 1997, ApJ, 483, 925

Crotts, A. P. S., Kunkel, W. E., & McCarthy, P. J. 1989, ApJ, 347, L61

Crotts, A. P. S., & Heathcote, S. R. 1991, Nature, 350, 683

———. 2000, ApJ, 528, 426

Cumming, R. J., & Lundqvist, P. 1997, in Advances in Stellar Evolution, ed. R. T. Rood (CUP:Cambridge), 297

Ensman, L., & Burrows, A. 1992, ApJ, 393, 742

Fitzpatrick, E. L. 1999, PASP, 111, 63

Fitzpatrick, E. L., & Walborn, N. R. 1990, AJ, 99, 1483

Fransson, C., Cassatella, A., Gilmozzi, R., Kirshner, R. P., Panagia, N., Sonneborn, G., Wamsteker, W. 1989, ApJ, 336, 429

Galavis, M. E., Mendoza, C., & Zeippen, C. J. 1997, A&AS, 123, 159

Garnavich, P. M., et al. 2000a, ApJ, submitted

Garnavich, P. M., Kirshner, R. P., & Challis, P. M. 2000b, IAU Circular No. 7360

Iping, R. C., Sonneborn, G., & Pun, C. S. J. 1999, BAAS, 31, 972

Jakobsen, P., et al. 1991, ApJ, 369, L63

Keenan, F. P., Hibbert, A., Ojha, P. C., & Conlon, E. S. 1993, Phys. Scripta, 48, 129

Khan, I. & Duerbeck, H. W. 1991, in ESO/EIPC Workshop: SN 1987A and Other Supernovae, ed. I. J. Danziger & K. Kjär (Garching: ESO), 251

Lawrence, S., & Crotts, A. 2000, IAU Circular No. 7359

Lawrence, S. S., Sugerman, B. E., Bouchet, P., Crotts, A. P. S., Uglesich, R., & Heathcote, S. 2000, ApJL, in press (astro-ph/0004191)

Lundqvist, P. 1999, ApJ, 511, 389

Lundqvist, P., & Fransson, C. 1996, ApJ, 464, 924

Lundqvist, P., & Sonneborn, G. 2000, in SN 1987A: Ten Years After, eds. M. Phillips & N. Suntzeff, A.S.P Conference Series (in press), astro-ph/9707144 (LS00)

Maran, S. P., Pun, C. S. J., & Sonneborn, G. 2000, IAU Circular No. 7359

Martin, C. M., & Arnett, D. A. 1995, ApJ, 447, 378

McKenna, F. C., Keenan, F. P., Kaler, J. B., Wickstead, A. W., Bell, K. L., & Aggarwal, K. M. 1996, PASP, 108, 610

Menzies, J. W. 1991, in ESO/EIPC Workshop: SN 1987A and Other Supernovae, ed. I. J. Danziger & K. Kjär (Garching: ESO), 209

Michael, E., et al. 2000, ApJ, submitted

Oppenheimer, B. D. 1999, Harvard University, senior thesis

Osterbrock, D. E. 1989, Astrophysics of Gaseous Nebulae and Active Galactic Nuclei (Mill Valley: University Science), 119

Panagia, N., Scuderi, S., Gilmozzi, R., Challis, P. M., Garnavich, P. M., & Kirshner, R. P. 1996, ApJ, 459, L17

Plait, P. C., Lundqvist, P., Chevalier, R. A., & Kirshner, R. P. 1995, ApJ, 439, 730

Podsiaklowski, P. 1992, PASP, 104, 717

Ramsbottom, C. A., Bell, K. L., & Stafford, R. P. 1996, Atomic Data Nucl. Data Tables, 63, 58

Sonneborn, G., et al. 1997, ApJ, 477, 848

Sonneborn, G., et al. 1998, ApJ, 492, L139

Stafford, R. P., Bell, K. L., Hibbert, A., & Wijesundera, W. P. 1994, MNRAS, 268, 816

Wampler, J., & Richichi, A. 1989, A&A, 217, 31

Wampler, E. J., Wang, L., Baade, D., Banse, K., D'Odorico, S., Gouiffes, C., & Tarenghi, M. 1990, ApJ, 362, L13

Wang, L. 1991, A&A, 246, L69

Wang, L., et al. 1996, ApJ, 466, 998